KeA1

CHINESE ROOTS
GLOBAL IMPACT

Contents lists available at ScienceDirect

Bioactive Materials

journal homepage: www.keaipublishing.com/en/journals/bioactive-materials





Bioactive superparamagnetic iron oxide-gold nanoparticles regulated by a dynamic magnetic field induce neuronal Ca²⁺ influx and differentiation

Elias Georgas ^{a,1}, Muzhaozi Yuan ^{b,1}, Jingfan Chen ^b, Ya Wang ^{b,c,d}, Yi-Xian Qin ^{a,*}

- a Department of Biomedical Engineering. The State University of New York at Stony Brook. Stony Brook. NY, United States
- ^b J. Mike Walker '66 Department of Mechanical Engineering, Texas A&M University, College Station, TX, United States
- ^c Department of Biomedical Engineering, Texas A&M University, College Station, TX, United States
- d Department of Electrical and Computer Engineering, Texas A&M University, College Station, TX, United States

ARTICLE INFO

Keywords:
Calcium influx
Membrane potential
Dynamic magnetic fields
Neuroregeneration
SPIO-Au Core-shell nanoparticles

ABSTRACT

Treating neurodegenerative diseases, e.g., Alzheimer's Disease, remains a significant challenge due to the limited neuroregeneration rate in the brain. The objective of this study is to evaluate the hypothesis that external magnetic field (MF) stimulation of nerve growth factor functionalized superparamagnetic iron oxide-gold (NGF-SPIO-Au) nanoparticles (NPs) can induce Ca^{2+} influx, membrane depolarization, and enhance neuron differentiation with dynamic MF (DMF) outperforming static MF (SMF) regulation. We showed the that total intracellular Ca^{2+} influx of PC-12 cells was improved by 300% and 535% by the stimulation of DMF (1 Hz, 0.5 T, 30min) with NGF-SPIO-Au NPs compared to DMF alone and SMF with NGF-SPIO-Au NPs, respectively, which was attributed to successive membrane depolarization. Cellular uptake performed with the application of sodium azide proved that DMF enhanced cellular uptake of NGF-SPIO-Au NPs via endocytosis. In addition, DMF upregulated both the neural differentiation marker (β 3-tubulin) and the cell adhesive molecule (integrin- β 1) with the existence of NGF-SPIO-Au NPs, while SMF did not show these effects. The results imply that noninvasive DMF-stimulated NPs can regulate intracellular Ca^{2+} influx and enhance neuron differentiation and neuroregeneration rate.

1. Introduction

Treating neurodegenerative diseases resulting from neuronal damage or degeneration is still the main clinical challenge due to the limited neuronal recovery ability and the slow speed of the neuroregeneration [1,2]. Among the strategies developed to promote axonal growth and neuron recovery, nanomagnetic actuation shows excellent potential to non-invasively stimulate neuronal differentiation and promote neuronal survival [3–6]. For example, static magnetic field (SMF) combined with superparamagnetic iron oxide nanoparticles (SPIO NPs) has been found to direct the neurite orientation along the magnetic force direction and promote neurite growth of PC-12 cells [7]. However, uncoated SPIO NPs result in instability in the neuronal environment [7–10], aggregations [11], and cellular toxicity [12–15], which leads to increased expression of inflammatory genes and decreased level of intracellular reduced glutathione [16]. The surface coating of SPIO NPs with gold (Au) can reduce toxicity and enhance cellular uptake due to its outstanding

biocompatibility [17–21], high stability [19,22], and tunable surface function [23]. Notably, the Au coating allows easy protein conjugation [24–26], such as nerve growth factor (NGF), through its stable amine binding affinity [27,28]. Our recent study demonstrated that the dynamic magnetic field (DMF) and NGF functionalized SPIO-Au NPs (NGF-SPIO-Au NPs) performed better than SMF by exhibiting the more enhancement of neuronal differentiation and neurite elongation of PC-12 cells [6]. However, the underlying mechanism of the stimulation effect by DMF and SPIO-Au NPs on neuronal differentiation and growth remains a question.

As Ca^{2+*} signaling plays a significant role in neuronal development, it is of great interest to explore how the nanomagnetic actuation by DMF and SPIO-Au NPs affect Ca²⁺ flux in PC-12 cells, which may trigger the Ca²⁺-mediated signaling pathways for the regulation of axonal growth and neuronal differentiation [29]. There are two possible mechanisms of nanomagnetic actuation on cell activities [30]: The first is that the rotation of DMF can exert a controllable and twisting force on NPs

Peer review under responsibility of KeAi Communications Co., Ltd.

^{*} Corresponding author. Department of Biomedical Engineering, The State University of New York at Stony Brook, Stony Brook, NY, United States. *E-mail address*: yi-xian.qin@stonybrook.edu (Y.-X. Qin).

 $^{^{1}\,}$ These authors contributed equally to this work.

attaching to the cell membrane, which leads to the cytoskeletal deformation of cells and the opening of mechanosensitive ion channels; The second is that magnetic NPs bounded to receptor complexes on the cell membrane can act as regulators to adjust the space between receptors under high-gradient magnetic field (MF) by pulling the receptors towards the MF direction, which can cause the receptor clustering and the downstream intracellular Ca²⁺ signaling. In addition, it is reported that the magnetic stimulated NPs attaching to the cell membrane can activate transmembrane receptors, which may trigger the local Ca²⁺ influx [31,32]. It is also found that SMF can trigger the amplitude increase of action potential in crayfish in an intensity and duration-dependent style [33]. This membrane depolarization by external stimuli may allow the Ca²⁺ to enter the neuron [5,34] and thus promote the neuronal survival [35] and the upregulation of neuronal specific gene/molecule [36]. However, it is still unknown whether or not the DMF and SMF differentially regulate the neuronal Ca²⁺ flux and how it is related to the action potential change of the neuronal membrane.

To evaluate the therapeutic activities of DMF-stimulated NPs, it is also important to investigate which cellular uptake mechanism is involved and whether DMF influences it. Cellular uptake pathways include specific or non-specific receptor-mediated endocytosis or the enhanced permeability and retention effect [37,38]. Factors such as NP characteristics, e.g., charge, surface modification, particle size, shape, and external stimulation, significantly affect intracellular uptake and distribution. So, it is necessary to understand these uptake mechanisms for each particular NP system [39-42]. Previous studies indicate that Au NPs are taken up by receptor-mediated endocytosis and are located in endosomes/lysosomes without entering mitochondria or nuclei [21, 43–45]. It is also reported that external SMF stimulation can strengthen the cellular uptake of SPIO NPs by enhancing the sedimentation process of NPs onto the cell membrane surface and that this promotional effect is dependent on MF intensity [46]. In addition, cellular uptake of SPIO-Au NPs into tumor cells was reported to be enhanced by SMF due to the magnetization of SPIO-Au NPs, which generate an attractive force to allow for the translocation through the cell membrane [47]. However, it remains a question whether or not the stimulation of DMF has a similar effect to SMF to enhance the delivery of NGF-SPIO-Au NPs into neurons and thus promote neuron differentiation and survival. Therefore in this work, we aim to study how the DMF-stimulated NGF-SPIO-Au NPs regulate neuronal Ca^{2+} flux and how it is related to an action potential change, as well as how it regulates NPs-neuron interactions, including cellular uptake rate.

2. Methods

2.1. Synthesis of NGF functionalized SPIO-Au NPs

The SPIO-Au NPs were synthesized according to our previous work [6,48]. In detail, a 10 nm Ferrotec EMG 304 SPIO cores (Ferrotec, EMG 304) were used and made at a dilution of 60 mM. Then after 5 min of sonication, 0.5 ml of the diluted SPIO NPs were mixed with deionized (DI) water at the volume of 19.5 ml to make the further diluted SPIO NPs at the concentration of 1.5 mM. Then 5.5 ml of this solution was mixed with sodium citrate (0.1 M) at an equal volume and stirred for 10 min to allow the exchange of absorbed OH- with citrate anions at the surface of SPIO NPs. Then this mixture was diluted to 100 ml by adding DI water. After that, 0.5 ml of HAuCl₄ solution (1%) was added to the mixture. Next, the pH value of the mixed solution was adjusted using NaOH solution (0.1 M) to make the final pH within 7-9. Then 0.6 ml of $NH_2OH^*HCl~(0.2~M)$ solution at the volume of 0.6 ml was added to the mixture to induce the formation of Au coating. During this process, the color of the solution was changed to pink-red in 5 min, indicating the appearance of the Au coating. In the end, the synthesized NPs were separated using magnetic decantation and washed with DI water three times. The as-synthesized SPIO-Au NPs were directly used in the following experiments without further purification. Chemicals used in

this section were purchased from Sigma-Aldrich (St. Louis, MO) unless otherwise stated.

A transmission electron microscope (TEM) was performed to examine the morphology of SPIO-Au NPs. SPIO-Au NPs in water solution was dropped onto a grid, which was dried and examined under TEM (80 kV). More than 100 NPs were measured to determine the average radii of SPIO-Au NPs. The zeta potential and hydrodynamic diameter of SPIO-Au NPs before and after NGF functionalization were measured using a Zetasizer apparatus (Malvern Instruments, UK). Triplicate measurements were performed. To verify the existence of Au in SPIO-Au samples, light absorbance spectra were recorded using a SHIMADZU UV-2450 spectrophotometer (Shimadzu Corp.). Inductively coupled plasma mass spectroscopy (ICP-MS) analysis was performed on a PerkinElmer NexION 300D ICP mass spectrometer to quantify the elemental composition of SPIO-Au NPs. SPIO-Au NPs were digested using aqua regia and diluted with 2% nitric acid and 1% hydrochloric acid before ICP-MS analysis. Triplicate samples were measured to get the average concentrations.

The functionalization of SPIO-Au NPs with NGF (N2513, Sigma) was performed by mixing 14 μg of NGF with 0.47 ml of SPIO-Au NPs (422 $\mu g/ml$) at a mass ratio of 1:14 (NGF: NPs). The mixture was then stirred for at least 3 h to allow sufficient functionalization at room temperature. Finally, the NPs functionalized with NGF were centrifuged and redispersed in DI water, denoted as NGF-SPIO-Au. (Final concentration of NGF-SPIO-Au NPs: 200 $\mu g/ml$).

2.2. PC-12 cell culture

PC-12 cells (from rat pheochromocytoma) obtained from American Type Culture Collection (ATCC) were cultured in ATCC-modified RPMI 1640 medium supplemented with 10% heat-inactivated horse serum (HS), 5% fetal bovine serum (FBS), and 1% penicillin-streptomycin (Gibco, Grand Island, NY). Cells were cultured in collagen type IV (C5533, Sigma-Aldrich, St. Louis, MO) and poly-L-lysine (P4707, Sigma-Aldrich, St. Louis, MO) coated Ibidi Petri dishes (D: 35 mm) in a humidified incubator under a 5% CO₂ atmosphere at 37 °C. To induce cell differentiation, PC-12 cells were incubated in serum-reduced media (1% heat-inactivated HS and 0.5% FBS).

2.3. DMF applicator

A Halbach array of magnets was designed, which provided a strong MF inside and near zero MF outside. The collection was designed for petri dish with a 38 mm inner diameter and printed by a 3D printer (Sindoh, 3DWOX 2X) using polylactic acid (PLA) filament. The magnetization direction of 8 different magnets (NdFeB, grade N52, the core strength of 1.48 T, dimensions $12.7 \times 12.7 \times 12.7$ mm, K&J Magnetics, Inc.) arranged around the circle was shown in Fig. 1A. A direct current (DC) motor was used to generate a rotation speed. An L298 N motor driver and the Arduino (Arduino nano) board were used to control DC motors (CQRobot 90:1) as illustrated in Fig. 1B. The L298 N is a dual H-Bridge motor driver which allows speed and direction control of two DC motors at the same time and is driven by a power supply (ALITOVE DC 12V). A potentiometer was used to control the rotation speed of the DC motor, and the speed can be read from the Arduino software, which created the DMF. In our previous study [6], the DMF applicator was designed for the petri dish to rotate inside the MF. Still, to eliminate centripetal force on the cells, the applicator was redesigned to allow the MF to turn around the petri dish. To determine the optimal rotation speed, Ca²⁺ influx was measured after 30 min of stimulation at frequencies of 0.1 Hz, 0.5 Hz, 1.0 Hz, and 1.5 Hz, and it was found that 1.0 Hz rotation resulted in the most significant Ca²⁺ influx (Fig. S1). Therefore, this rotation speed was used for the remainder of the experiments.

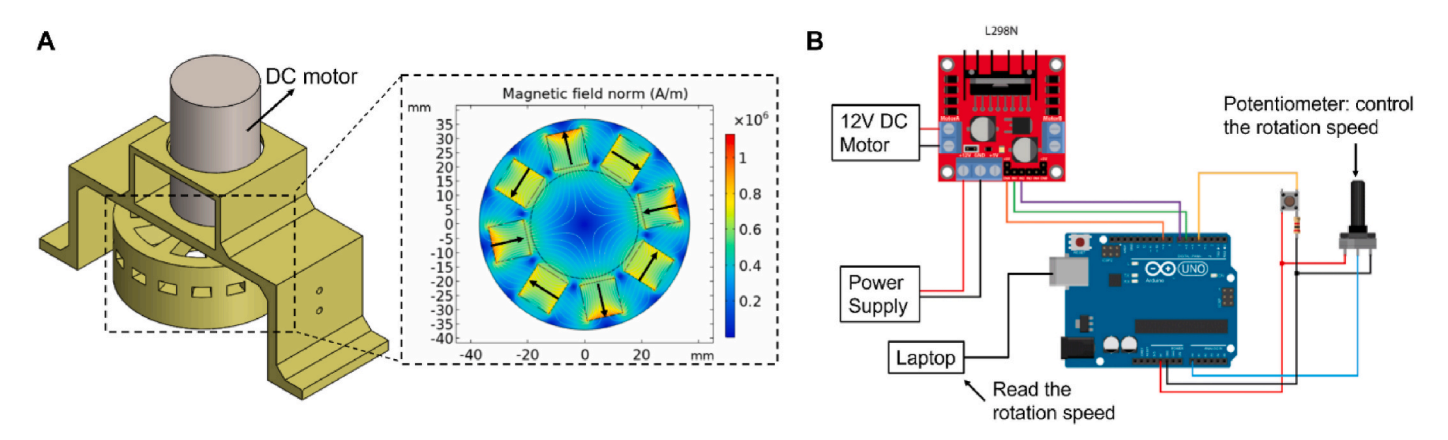


Fig. 1. Dynamic magnetic applicator setup. (A) The Halbach array of magnets driven by a DC motor and its magnetic flux diagram (simulated from COMSOL). (B) The construction of the DC motor driven by L298 N and Arduino.

2.4. Ca^{2+} influx imaging

PC-12 cells were seeded at 2×10^5 cells/dish in collagen type IV and poly-L-lysine coated 35-mm glass bottom dishes until 80% confluency. The cell growth medium was switched to a serum-reduced medium to induce differentiation for 48 h. After 48-h incubation in the serumreduced medium, cells were treated with NGF-SPIO-Au NPs at a concentration of 20 ug/ml in the serum-reduced medium for 48 h to allow the NPs to interact with the cells. Four groups were evaluated for Ca²⁺ influx: (1) Control: NPs only, (2) SMF + NPs, (3) 1 Hz DMF, (4) 1 Hz DMF + NPs. Before the MF application, cells were incubated with the Fluo-4 direct calcium assay (Life Technologies) according to the manufacturer's protocol to detect intracellular Ca²⁺ flux. In brief, 10 ml of calcium assay buffer and 200 µL of the 250 mM probenecid stock solution were mixed with the calcium reagent. The calcium reagent solution was then directly added to the dishes in a 1:1 ratio for 1 h before fluorescence imaging. For the MF stimulation, cells receiving either SMF or 1 Hz DMF were stimulated for 30 min, and then the Ca²⁺ level was monitored for 3 min after the removal of MF stimulation. The control group went through the same procedure but without MF stimulation. The Ca²⁺ signals of PC-12 cells were captured by performing real-time confocal imaging on Zeiss LSM 510 META NLO Two-Photon Laser Scanning Confocal Microscope System (Carl Zeiss Inc. Jena, Germany) with 40x objectives under 488-nm laser excitation at the speed of 2 frames/second (512 \times 512-pixel images). Five active cells with Ca²⁺ influx within each field of view were selected, and fluorescence intensities of the cells were quantified using LSM Image Browser software (Version 4.2, Carl Zeiss, Germany). The measured fluorescence signals. F, were normalized to the baseline fluorescence intensity F_0 (10 s). Further analysis was performed to obtain the total fluorescence over the 3 min of imaging by calculating the area under the curve (AUC). The AUC was normalized to line y = 1 using the integral, f(x) - 1dx, where f(x)is equal to the normalized fluorescence curve Eq. (1,2). F₀ is the baseline fluorescence intensity; and $\Delta F/F_0$ is the fluorescence change at cell membrane.

$$AUC = \int \mathbf{1}f(\mathbf{x}) - \mathbf{1}d\mathbf{x} \tag{1}$$

$$f(x) = \Delta F/F_0 \tag{2}$$

2.5. Membrane potential measurement

PC-12 cells were subjected to the same conditions as mentioned above for the membrane potential experiment. Four groups were evaluated for membrane potential change: (1) Control: NPs, only, (2) SMF + NPs, (3) 1 Hz DMF, (4) 1 Hz DMF + NPs. Before MF application, cells were incubated with FluoVoltTM membrane potential kit (Life

Technologies) according to the manufacturer's protocol to detect membrane potential change. In brief, FluoVoltTM loading solution was prepared by mixing 100 μ L of 100x PowerLoadTM concentrate, 10 μ L of FluoVoltTM dye, and 10 mL of 20 mM glucose in a live cell imaging solution (LCIS) (Life Technologies). Then, 2 mL of FluoVoltTM loading solution was added to cells and incubated at room temperature for 30 min. Next, cells were washed with LCIS, and then 2 mL of 20 mM Glucose in LCIS was added for live cell imaging using the same methodology and equipment described above for the Ca²⁺ influx imaging. The measured fluorescence signals, F, were normalized to the baseline fluorescence intensity F₀ (10 s), and the cell membrane's change in F (Δ F/F₀) was determined for 1 min following 30 min of MF application. AUC of the Δ F/F₀ traces was determined using the trapezoidal method.

2.6. TEM and ICP-MS analysis-cellular uptake pathway

To determine the cellular uptake mechanism of NGF-SPIO-Au NPs in the presence of DMF, PC-12 cells were seeded onto a type IV collagen, and poly-L-lysine coated Aclar® (Electron Microscopy Sciences Inc.) film in a 35-mm dish at a density of 2 $\times\,10^5$ cells per dish until 80% confluency. The medium was switched to a serum-reduced medium to induce differentiation for 48 h. After 48-h incubation in the serumreduced medium, cells were treated with NGF-SPIO-Au NPs at a concentration of 20 μ g/ml in the serum-reduced medium for 48 h to allow the NPs to interact with the cells. Sodium azide (NaN3) (10 mM) was added to the cells before 30 min of 1 Hz DMF treatment to block endocytosis of the NGF-SPIO-Au NPs. Three groups were tested: (1) Control: NPs only, (2) 1 Hz DMF + NPs, (3) 1 Hz DMF + NPs + NaN₃. After 30 min of DMF treatment, cells were prefixed in 2.5% electron microscopy grade glutaraldehyde and 1.5% paraformaldehyde in 0.1 M phosphate buffer at room temperature for 1 h. Samples were then washed with 0.1 M phosphate buffer, followed by post-fixation with 1% osmium tetroxide solution, gradual dehydration with ethanol and acetone infiltration, and embedded in Embed 812 resin. Ultramicrotome (EM UC7, Lecia) was used to section thin specimens at the thickness of 60 nm 1% uranyl acetate was used to post-stain thin section specimens before TEM imaging. Specimens were characterized by using TEM (JEM1400, JEOL) at the accelerating voltage of 80 kV. To quantitatively evaluate the cellular uptake rate of NPs under DMF, ICP-MS analysis was performed to measure gold content. PC-12 cells underwent the same experimental procedure described above for the TEM analysis. After the cells underwent 30 min of DMF treatment, the cells were washed 3 times with serum-reduced media to remove unassociated, unattached, or free NPs outside the cells. The cells were then gently detached from the plate and collected in a 1.5 ml centrifuge tube. A trypan blue exclusion assay was run to calculate the amount of cells in each sample before the cells were digested using aqua regia. Samples

were diluted using 2% nitric acid and 1% hydrochloric acid to signal match mixed calibration standards. Gold concentration analyses were performed on an Agilent 7500cx quadrupole ICP-MS. Unknown concentrations were calculated based on standard calibration curves, with standards frequently run between unknowns to monitor for drift in signal intensity.

2.7. RNA extraction and reverse transcription-polymerase chain reaction (RT-PCR)

PC-12 cells were seeded in type-IV collagen, and poly-L-lysine coated 35-mm dishes at a density of 2×10^5 cells/dish. After reaching confluency, cells were incubated with fresh serum-reduced medium for 48 h to induce differentiation. Cells were then incubated with either SPIO-Au NPs, NGF, or NGF-SPIO-Au NPs in the presence or absence of SMF/DMF. A negative control group was included that had cells without NPs, NGF or MF. Cells were treated for 30 min with either SMF or 1 Hz DMF. Total mRNA was extracted from the PC-12 cells using TRIzol® Reagent (Invitrogen) and 1-bromo-3choloropropane. mRNA concentration of each sample was measured using a NanoDrop 2000c Spectrophotometer (NanoDrop Technologies, LLC, Wilmington, Delaware). All mRNA samples were diluted to 10 ng/µl and then reverse transcribed to complementary DNA using TaqMan® reverse transcription reagents (Applied Biosystems). Polymerase chain reaction amplification was completed using SYBR Green on a StepOnePlus Real-Time PCR System (Applied Biosystems) to determine the gene expression of integrin-β1 and \beta3-tubulin. The expression levels were recorded concerning the negative control group and were normalized β-actin gene expression using the $2^{-\Delta\Delta CT}$ method. Primers used are shown in Table 1 (Integrated DNA Technologies).

2.8. Neurite growth evaluation

To evaluate neurite growth, PC-12 cells were seeded in type-IV collagen and Poly-L-Lysine coated 35-mm dishes at 2×10^5 cells/dish density. After reaching confluency, cells were incubated with fresh serum-reduced medium for 48 h to induce differentiation. Cells were then incubated with NGF-SPIO-Au NPs, DMF, NPs + DMF and NPs + SMF. Next, cells were treated for 30 min with either SMF or 1Hz DMF. After 30 min of treatment, the cells were fixed with 4% paraformaldehyde, and a light microscope (Axiovert 200 M, Carl Zeiss, USA) was used to take the images of PC-12 cells. For each sample, more than 200 cells were quantified for the neurite number and number of differentiated cells.

2.9. Statistical analyses

All results were analyzed based on at least 3 independent experiments and expressed using standard deviation. Statistical analysis was performed by the one-way analysis of variance with Tukey post hoc test. RT-PCR results were analyzed by two-way analysis of variance with Tukey post hoc test. P value less than 0.05 was considered as a significant difference (GraphPad Prism version 6.01, San Diego, California).

Table 1Primers used for quantitative real-time PCR.

Gene	Forward (F) and reverse (R) primer sequence-(5"-3')	
β-Actin	F: TGACGTTGACATCCGTAAAG	
	R: AGGAGCCAGAGCAGTAAT	
Integrin-β1	F: TGGTCAGCAACGCATATC	
	R: TTACATTCCTCCAGCCAATC	
β3-Tubulin	F: GGCCTCCTCTCACAAGTAT	
	R: GCCTGAATAGGTGTCCAAAG	

3. Results

In this work, we hypothesized that the DMF stimulated NGF-SPIO-Au NPs cause a change in membrane potential, which triggers the opening of Ca2+ channels located at the membrane and the increase of intracellular Ca²⁺ flux. To test this hypothesis, we first visualized the Ca²⁺ flux using Fluo-4 and compared the effect of SMF and DMF at the frequency of 1 Hz in the presence and absence of NGF-SPIO-Au NPs. We then studied how the membrane potential was changed under each condition. To unveil the mechanism of DMF-stimulated SPIO-Au NPs regulating Ca²⁺ flux and action potential, the cellular uptake study was performed to reveal the interaction between NPs and PC-12 neuron-like cells. The RT-PCR analysis was performed to explore how neuronal differentiation was affected by evaluating the expression of neuronal differentiation-related genes and cell adhesive molecules. This work demonstrates the potential for nanomagnetic actuation of NGF-SPIO-Au NPs using 1 Hz DMF as a non-invasive neuron stimulation technique for neuron regeneration.

3.1. Material characterization

The TEM images of as-synthesized SPIO and SPIO-Au NPs are shown in Fig. 2(A-D). The radii of SPIO NPs as core materials and SPIO-Au NPs were measured to be 6.2 \pm 0.8 nm and 7.5 \pm 1.5 nm, respectively. SPIO-Au NPs exhibited quasi-spherical shapes in TEM images. As shown in Fig. 2 (E), the high-resolution TEM image exhibited the lattice fringes with a spacing close to 0.24 nm, corresponding to the Au (111) lattice, which confirmed the existence of Au at the surface of SPIO NPs. The formation of Au shell at the surface of SPIO was also confirmed by UV-Vis light absorption spectrum measurement, which identified its characteristic surface plasmon resonance (SPR) peak at 523 nm, as shown in Fig. 3A. The magnetic response of SPIO-Au NPs and the existence of SPIO was confirmed by using an external magnet to successfully attract SPIO-Au NPs towards the direction of the MF, as shown in Fig. 3B and C. The existence of both iron and gold in the SPIO-Au sample was confirmed by ICP-MS analysis with the elemental ratio of Fe/Au to be 39/61, as shown in Table 2. As shown in Table 3, the zeta potential of SPIO-Au NPs before and after NGF functionalization was $-32.1\,\pm\,1.5$ and -18.4 ± 3.0 mV; the hydrodynamic diameter of SPIO-Au NPs before and after NGF functionalization was 53.8 \pm 0.3 and 63.0 \pm 1.1 nm. The results suggested the successful functionalization of NGF onto SPIO-Au

3.2. DMF stimulated SPIO-Au NPs to trigger intracellular Ca²⁺ flux

To demonstrate whether SMF and DMF differentially induce Ca²⁺ influx in differentiated PC-12 cells with NGF-SPIO-Au NPs, the Ca²⁺ signal in cell body was visualized using confocal microscopy. Results showed a decrease in fluorescence intensity for PC-12 cells treated with NGF-SPIO-Au NPs alone (Fig. 4A), while 30 min treatment of SMF + NGF-SPIO-Au NPs, 1 Hz DMF alone, and 1 Hz DMF + NGF-SPIO-Au NPs (Fig. 4B-D, respectively) resulted in increases in fluorescence intensity with 1 Hz DMF + NGF-SPIO-Au NPs being the most pronounced. To further quantify the fluorescence change, the F/F0 (normalized fluorescence by baseline fluorescence) in cell body was plotted (Fig. 4E). After 30 min of MF treatment, there was an increase in fluorescence signal compared to baseline in all MF treated groups with 1Hz DMF + NPs enhancing Ca²⁺ influx the greatest. On the other hand, neurons with NPs alone resulted in a decrease in fluorescence signal, further corroborating the qualitative confocal images. To further compare the changes in Ca^{2+} influx fluorescence, the area under the $\Delta F/F_0$ curve was determined and normalized to the baseline area of the line y = 1 (Fig. 4F). 1 Hz DMF treatment in the presence or absence of NGF-SPIO-Au NPs resulted in significantly greater total intracellular Ca²⁺ influx than NPs alone (P < 0.05 and P < 0.0001, respectively) while there was no significant increase following SMF + NPs treatment compared to NPs

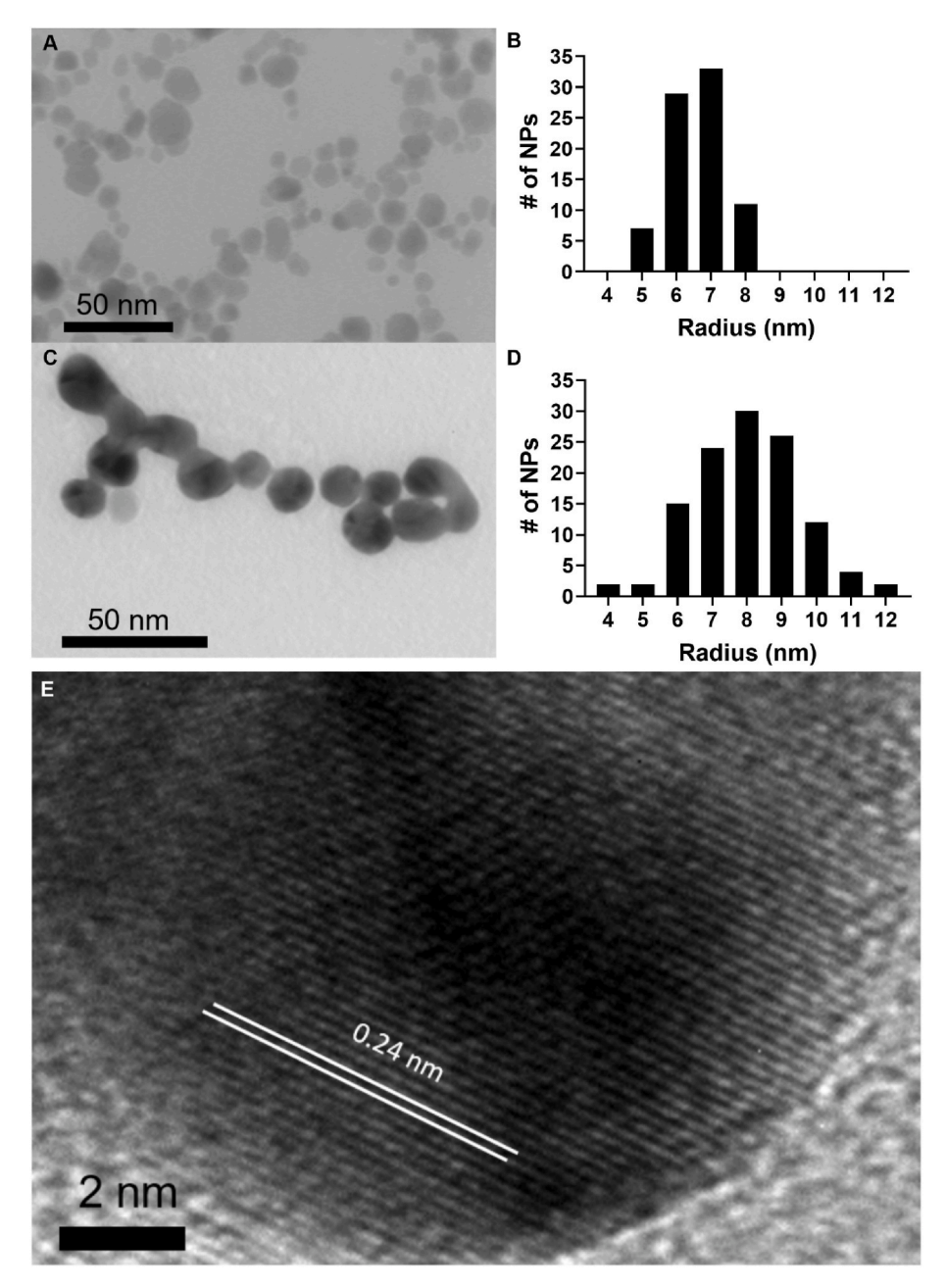


Fig. 2. TEM images of (A) SPIO NPs; (B) Histogram showing the size distribution of SPIO; (C) SPIO-Au NPs (D) Histogram showing size distribution of SPIO-Au NPs. and (E) TEM image of SPIO-Au NPs showing the lattice fringe of Au (111).



Fig. 3. Light absorbance of SPIO-Au NPs with the characteristic SPR peak at 523 nm (A) Photographs showing SPIO-Au NPs without magnet (B) and with a magnet (C) showing the movement of SPIO-Au NPs along the magnet direction.

Table 2ICP-MS results of the relative mass composition of Au and Fe in SPIO-Au NPs. (Assuming the total mass of Au and Fe equals to 1).

Sample name	Fe/%	Au/%
SPIO-Au	39 ± 4	61 ± 4

Table 3Zeta potential and hydrodynamic diameter of SPIO-Au NPs before and after NGF functionalization.

	Zeta potential (mV)	Hydrodynamic diameter (nm)
SPIO-Au	-32.1 ± 1.5	53.8 ± 0.3
SPIO-Au-NGF	-18.4 ± 3.0	63.0 ± 1.1

alone. In addition, 1 Hz DMF + NPs resulted in a significant increase in total intracellular Ca^{2+} influx than 1 Hz DMF alone and SMF+NPs (P < 0.001 and P < 0.0001, respectively) while there was no significant difference between 1 Hz DMF and SMF + NPs treatments.

3.3. DMF and SMF differentially regulate membrane potential

To elucidate whether SMF or DMF treatment differentially regulate membrane potential of PC-12 cells, the localized membrane potential was visualized using confocal microscopy by employing FluoVoltTM membrane potential kit. An increase in fluorescence indicates depolarization, while a decrease indicates hyperpolarization. The $\Delta F/F_0$ (normalized by baseline fluorescence) of the cell membrane was plotted in Fig. 5A. SMF treatment in the presence of NGF-SPIO-Au NPs resulted in a decrease in fluorescence, indicating hyperpolarization, while 1 Hz DMF treatment in the presence or absence NGF-SPIO-Au NPs resulted in fluctuations of depolarization and hyperpolarization compared to control. NGF-SPIO-Au NPs treatment alone maintained the membrane potential at the baseline. Further quantification of total membrane fluorescence change by determining the area under the $\Delta F/F_0$ curve revealed SMF stimulation of NGF-SPIO-Au NPs resulted in a significant decrease in total membrane potential change compared to NPs alone, 1 Hz DMF alone, and 1 Hz DMF + NPs (P < 0.001) (Fig. 5B). On the other hand, there were no significant differences in total membrane potential change between NPs alone, 1 Hz DMF alone, and 1 Hz DMF + NPs. These results demonstrate a differential effect of SMF vs DMF on neuron membrane potential.

3.4. Cellular uptake of DMF stimulated NPs: TEM and ICP-MS analysis

The cellular uptake mechanism of 1 Hz DMF stimulated NGF-SPIO-Au NPs was examined by TEM and ICP-MS analysis on PC-12 cells following 30 min of DMF treatment in the presence or absence of NaN₃. Cells incubated with NGF-SPIO-Au NPs alone showed NP cluster congregation at the cellular membrane with no internalization occurring (Fig. 6A&B). While TEM images showed internalization of NPs, located inside the endosomal vesicles in the cytoplasm following DMF treatment (Fig. 6C&D), suggesting the promotional effect of DMF on enhancing the cellular uptake of NGF-SPIO-Au NPs. The addition of NaN3, an endocytosis blocker, resulted in the inhibition of DMF-treated NPs to be internalized inside the cells, further demonstrating energy-dependent endocytosis as the primary uptake mechanism of DMF-treated NPs (Fig. 6E&F). In addition, the cytoplasmic membranes remained intact for all groups. Also, quantification of gold content via ICP-MS analysis revealed a significant increase in the cellular uptake rate of NGF-SPIO-Au NPs following DMF treatment compared to cells incubated with NGF-SPIO-Au NPs alone (P < 0.05) (Fig. 7). Furthermore, the treatment of NaN3 significantly inhibited the cellular uptake rate of NGF-SPIO-Au NPs with DMF, suggesting the energy-dependent endocytic pathway of NGF-SPIO-Au NPs as the primary uptake mechanism (P < 0.001)

(Fig. 7), which is in accordance with TEM results.

3.5. DMF enhances neuronal differentiation of PC-12 cells

RT-PCR was used to quantify the effect of SMF and 1 Hz DMF in the presence of NPs, NGF, and NPs + NGF on the expression level of the adhesive molecule, integrin-β1, and the neural-specific marker, β3tubulin, in PC-12 cells. SMF and DMF stimulation of SPIO-Au NPs resulted in a slight upregulation of integrin-β1 expression, but this effect was not significantly different from NPs alone (Fig. 8A). However, DMF stimulation of SPIO-Au NPs significantly upregulated β3-tubulin expression compared to NPs alone and SMF + NPs (P < 0.01 and P <0.001, respectively) (Fig. 8A), while there was no significant difference between SMF + NPs and NPs alone. In addition, SMF and DMF stimulation in the presence of NGF resulted in no significant upregulation of integrin- $\beta 1$ expression compared to NGF alone while DMF stimulation in the presence of NGF significantly increased β3-tubulin expression compared to SMF + NGF and NGF alone (P < 0.001, and P < 0.0001, respectively) (Fig. 8B). No significant difference in β3-tubulin expression was found between SMF + NGF and NGF alone. Furthermore, DMF stimulation of NGF-SPIO-Au NPs resulted in a significant upregulation of integrin- β 1 expression compared to NGF-SPIO-Au NPs alone (P < 0.05), while there was no significant difference in integrin-β1 expression between SMF and DMF stimulation (Fig. 8C). On the other hand, SMF and DMF stimulation of NGF-SPIO-Au NPs significantly upregulated β3tubulin expression compared to NGF-SPIO-Au NPs alone (P < 0.01 and P < 0.05, respectively) while there was no significant upregulation of β3-tubulin expression between SMF and DMF stimulations. The results suggested that DMF enhanced the β3-tubulin expression for all three cases: NP, NGF, and NP + NGF. Interestingly, DMF + NGF resulted in a significant upregulation in β 3-tubulin expression compared to DMF +NP + NGF and SMF + NGF (P < 0.05 and P < 0.0001, respectively) but was not significant compared to SMF + NP + NGF (Fig. 8D). However, there were no significant differences in integrin-β1 expression between these groups (Fig. 8D). In addition, morphologic analysis of differentiated cells showed that the ratio of differentiated cells is significantly increased by DMF + NP + NGF and SMF + NP + NGF (Fig. 9A), compared to the group without MF or NPs, suggesting the effect of MF on enhancing neuronal differentiation. While the number of neurites per differentiated cells did not show a significant change in all groups (Fig. 9B). These results demonstrate that DMF is the key factor that enhances neuronal differentiation in the presence of NPs, NGF, and NGFconjugated NPs.

4. Discussion

External noninvasive SMF applied to SPIO NPs as a nanocarrier of NGF has been shown to stimulate neurite outgrowth and our previous work has demonstrated that DMF was able to further enhance neurite outgrowth compared to SMF [6,7,49–51]. However, the effect of DMF and SMF on ${\rm Ca^{2+}}$ influx and how it's related to membrane potential to induce neuron differentiation and outgrowth is still a question, which is essential to understand the stimulatory effects seen in previous studies. In this work, we investigated the differential effects of SMF-stimulated NGF-SPIO-Au NPs compared to DMF stimulation in the presence or absence of NGF-SPIO-Au NPs on ${\rm Ca^{2+}}$ influx and membrane potential and how this affects neuron differentiation. We demonstrated that 1 Hz DMF-stimulated NGF-SPIO-Au NPs enhanced ${\rm Ca^{2+}}$ influx by 300% and 535% compared to DMF alone, and SMF-stimulated NGF-SPIO-Au NPs, respectively because of successive depolarizations, which led to upregulation of neuronal gene expression.

Changes in intracellular Ca^{2+} concentration are key regulators of cellular function in that hundreds of proteins can bind Ca^{2+} and consequently change their activity, which can induce gene transcription and influence mRNA translation and even post-translation protein modifications [52,53]. Tay et al. found that SMF stimulation with

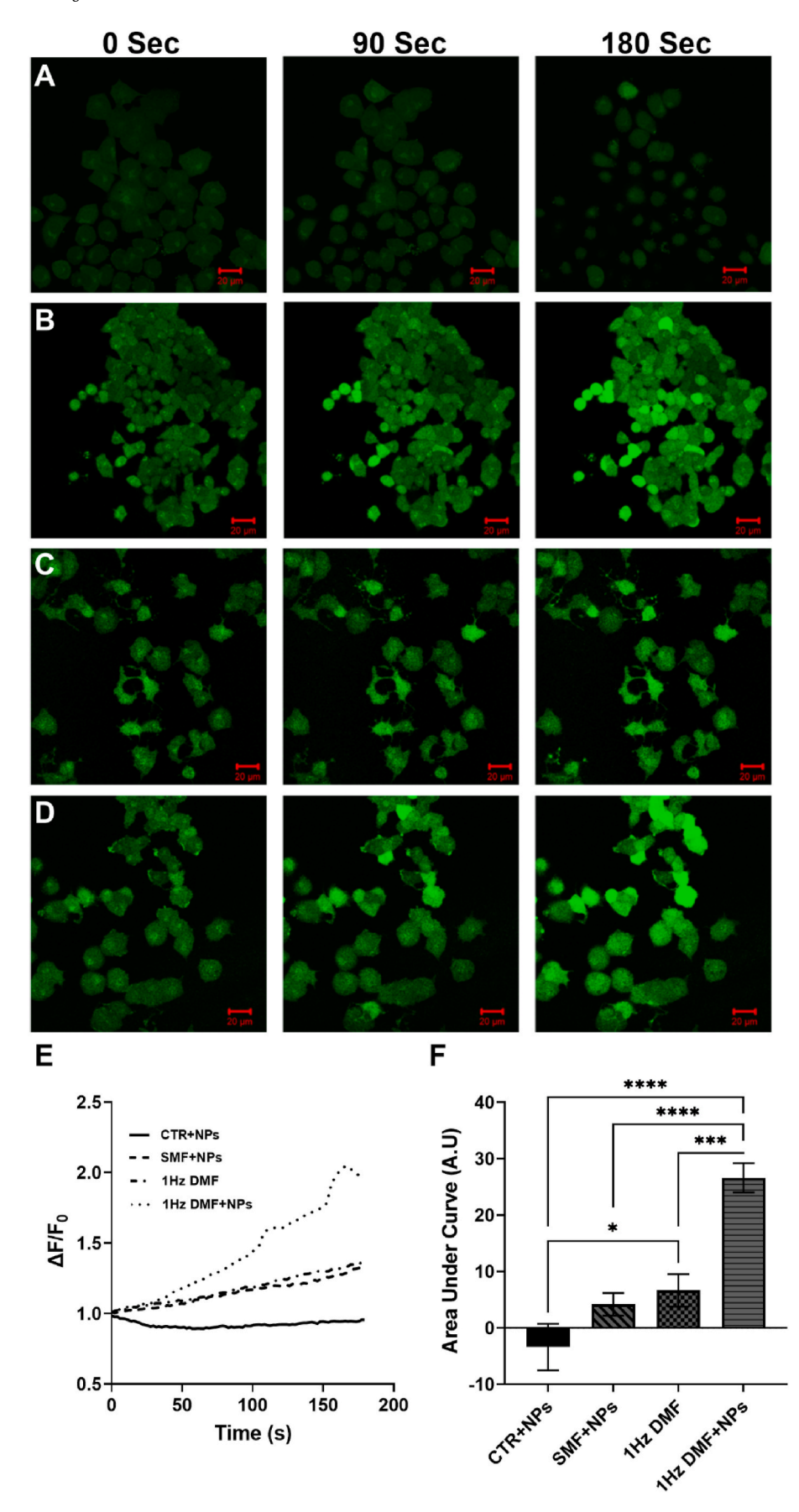


Fig. 4. Ca²⁺ influx of PC-12 Cells increased following 30 min of 1 Hz DMF treatment in the presence of NGF-SPIO-Au NPs. Changes in Ca²⁺ influx in (A) Control (NPs only), (B) SMF + NPs, (C) 1 Hz DMF, (D) 1 Hz DMF + NPs at 0, 90, and 180 s post treatment. Scale bar: 20 μm . (E) The average change in intracellular Ca²⁺ fluorescence 3 min following magnetic field treatment. (F) Total intracellular Ca²⁺ fluorescence determined by the area under curve analysis reveals enhanced Ca²⁺ influx following different MF treatments. *P < 0.05, ***P < 0.001, ****P < 0.0001.

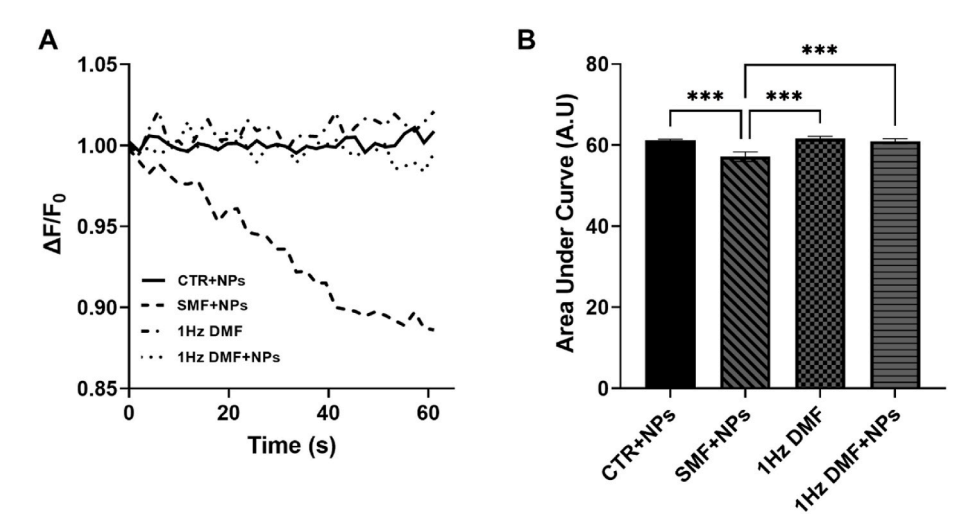


Fig. 5. DMF and SMF differentially regulate membrane potential. (A) The average change in membrane potential fluorescence 1 min following magnetic field treatment. (B) Total change in membrane potential fluorescence determined by the area under curve analysis reveals hyperpolarization from SMF and slight depolarization from DMF treatment. ***P < 0.001.

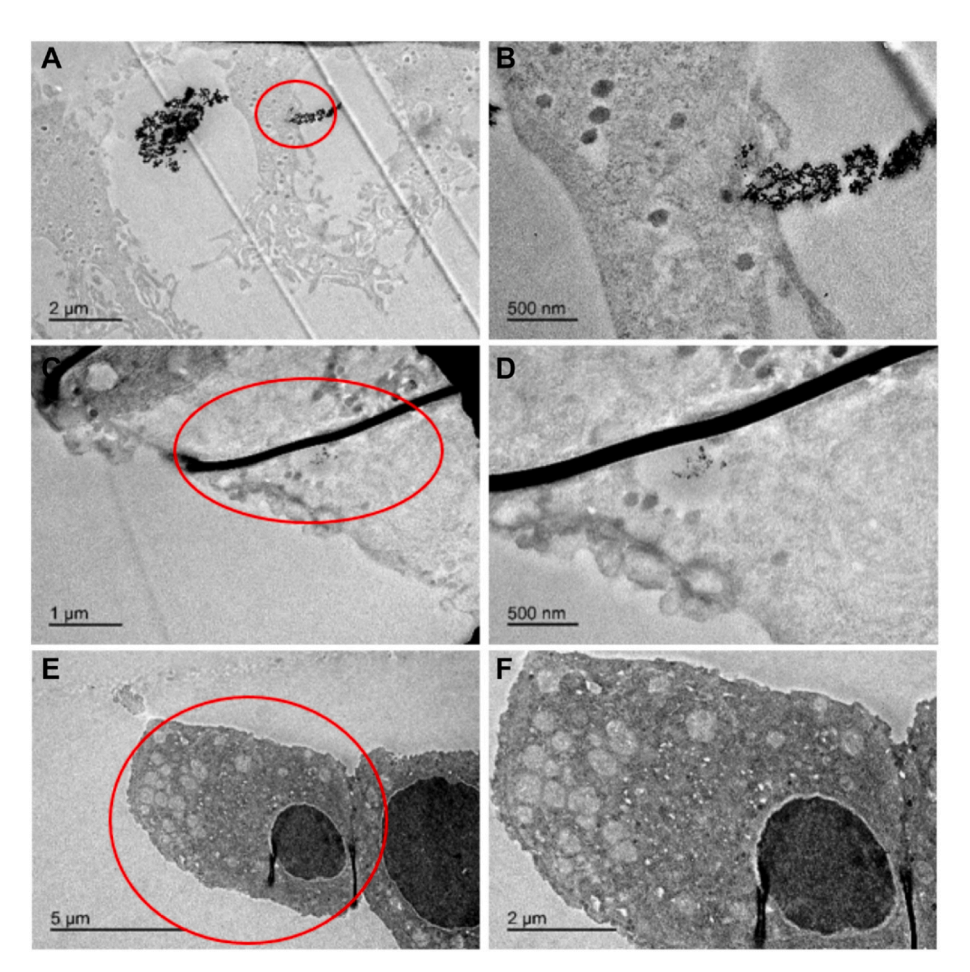


Fig. 6. Cellular uptake analysis via TEM. (A) and (B) PC-12 cells treated with NGF-SPIO-Au NPs only; (C) and (D) PC-12 cells treated with NGF-SPIO-Au NPs and 1 Hz DMF; (E) and (F) PC-12 treated with NGF-SPIO-Au NPs, 10 mM sodium azide, and 1 Hz DMF. (B), (D), and (F) Enlarged images of areas shown inside the circles in (A), (C), and (E), respectively.

ferromagnetic NPs triggered Ca^{2+} influx in cortical neural networks with a 20% increase in Ca^{2+} fluorescence signals and that N-type mechano-sensitive Ca^{2+} channels play a key role in this change in intracellular Ca^{2+} level [54,55]. Our results demonstrated a similar increase in Ca^{2+} influx after SMF stimulation, suggesting that N-type

mechano-sensitive Ca^{2+} channels may be the key regulator of Ca^{2+} influx. Interestingly, DMF stimulation in the absence of NGF-SPIO-Au NPs resulted in an increase in Ca^{2+} influx, suggesting that DMF may differentially regulate Ca^{2+} channels compared to SMF. Grassi et al. found that electromagnetic fields (50Hz, 1.0 mT) did not affect the

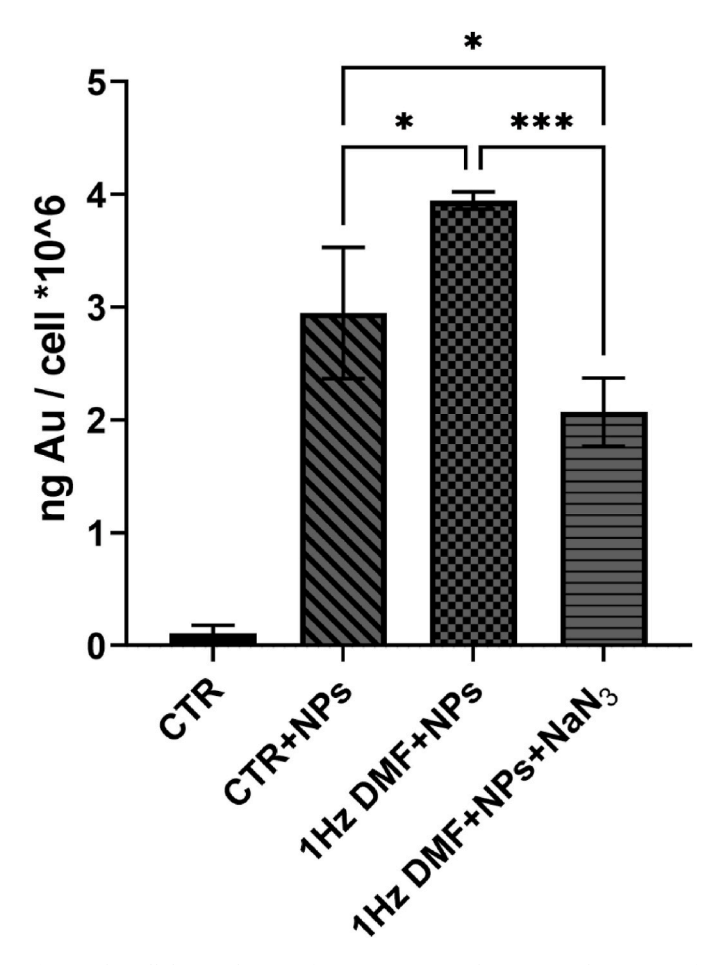


Fig. 7. The cellular uptake rate of NGF-SPIO-Au NPs by ICP-MS. The amount of Au (ng) per cell of PC-12 cells was quantified for the following groups: treated with NGF-SPIO-Au NPs only; NGF-SPIO-Au NPs and 1 Hz DMF; NGF-SPIO-Au NPs, 10 mM sodium azide, and 1 Hz DMF. A control group with no NPs was used to show relatively no Au was in cells. $^{*}P < 0.05$, $^{***P} < 0.001$.

gating of L- and N-type voltage-gated Ca2+ channels in neurons, but enhanced the expression of Ca^{2+} channel subunit α_1 , indicating an increase in the amount of active Ca²⁺ channels which resulted in an increase in Ca²⁺ influx [56]. Furthermore, MFs (50 Hz, 1.0 mT) enhanced intracellular Ca²⁺ levels evidenced by c-fos expression and more elongated mature neurites in human neural progenitor cells, which were neutralized by blocking N-methyl-D-aspartate (NMDA) receptors, indicating that NMDA receptors may be a key player in the MF enhancement of neural activity [57]. In addition, DMF stimulation in the presence of NGF-SPIO-Au NPs resulted in the greatest Ca²⁺ influx, which may be due to the combined stimulatory effect from SMF-NPs and DMF: the twisting force on NPs led to the opening of mechanosensitive ion channels such as Piezo 1/2 and clustering of bounded receptor complexes such as TrkA and NMDA. What is more, the Ca²⁺ regulation by DMF and SPIO-Au NPs suggested the universal application of this stimulation method on other mechano-sensitive ion channels, such as mechanosensitive K⁺ channel (TREK-1) [58] and Ca²⁺/K⁺ pump [59]. These channels can be stimulated by either magnetic NPs or MF as reported before.

Cell membrane potential is determined by ionic permeability that can modulate intracellular ${\rm Ca^{2+}}$ concentration and these changes further regulate the cell growth [60]. Therefore, it is important to understand how membrane potential is affected by external MFs in the presence of NPs to support their related biomedical applications. We found that DMF stimulation in the presence or absence of NGF-SPIO-Au NPs resulted in fluctuations of depolarization and hyperpolarization, which led to a sustained increase in ${\rm Ca^{2+}}$ influx. However, SMF

stimulation of NGF-SPIO-Au NPs induced membrane hyperpolarization, which limited the increase in Ca²⁺ influx. Mclean et al. found that adult mouse dorsal root ganglion neurons elicited action potentials inhibited by SMF, indicating that SMF may alter the ability of neurons to depolarize, which was demonstrated in our study [61]. In addition, the charge of the NPs may influence membrane potential. Arvizo et al. found that positively charged Au NPs induced membrane depolarization of two ovarian cancer cells (CP70, A2780), human bronchial epithelial cells, and human airway smooth muscle cells, while negatively charged Au NPs had a negligible effect on membrane depolarization [60]. The NGF-SPIO-Au NPs used in this study have a zeta potential of -18.4 mV, which may be a key indicator of the differential membrane potentials seen under SMF and DMF. The hyperpolarization seen with SMF stimulation may be due to an increased uptake of NPs under a uniform MF gradient, resulting in an accumulation of negative charge within the cell and thus inducing hyperpolarization. On the other hand, DMF creates a rotating MF gradient which can drive the NPs to move in and out of the cell, resulting in fluctuation of depolarization and hyperpolarization and increased Ca²⁺ influx compared to SMF.

The TEM and ICP-MS analysis revealed that DMF enhanced cellular uptake of NGF-SPIO-Au NP, mediated by endocytosis. Cells incubated with NGF-SPIO-Au NPs accumulated at the cell membrane with no internalization while stimulating them with DMF resulting in considerable cellular uptake of NGF-SPIO-Au NPs in endosomal vesicles. Blocking endocytosis using sodium azide resulted in no NPs at the cell membrane or cytoplasm, indicating endocytosis as the primary uptake mechanism. To further identify which endocytic uptake pathways are utilized, additional inhibitors such as chlorpromazine, filipin III, and amiloride will be used to inhibit clathrin-mediated endocytosis, caveolae, and micropinocytosis, respectively in future studies [62].

In addition, we found from the molecular analysis that DMF stimulation in the presence of NPs, NGF, and NP + NGF upregulated neuronalspecific markers as well as the cell adhesive molecules, which were associated with the cell attachment and neurite growth. And that this stimulation effect was less significant under SMF stimulation. These results suggest that the nanomagnetic actuation by DMF induces membrane depolarization followed by enhanced Ca²⁺ influx to induce transcription of neuronal genes for enhanced differentiation and outgrowth. MF stimulation (50 Hz, 1 mT) has been shown to increase β3-tubulin, MAP2, and TUJ1 expression in neural stem cells due to enhanced Ca²⁺ influx and Ca²⁺ channel expression [56,57,63]. In addition, MF stimulation enhanced neural proliferation and inhibited puromycin- and H₂O₂-induced apoptosis, which was counteracted by Ca²⁺ channel blockage, indicating that Ca²⁺ signaling is a key factor in the neuroregeneration rate [56]. Our results demonstrated an increased neuroregeneration rate, which was induced by the increase in Ca²⁺ influx following DMF stimulation.

Interestingly, DMF in the presence of NGF alone significantly upregulated \(\beta \)-tubulin expression compared to DMF-stimulated NGF-SPIO-Au NPs and SMF in the presence of NGF but was not significant compared to SMF-stimulated NGF-SPIO-Au NPs. Indeed, DMF is the most important factor for enhanced neuronal differentiation, which may be attributed to increases in slow and rapid endocytosis, endocytosis overshoot, and bulk endocytosis as a result of increased calcium influx through P/Q and N-type calcium channels previously seen under 50 Hz MF [64]. The increase in endocytosis under DMF can enhance the uptake of NGF into cells and thus promote neuronal differentiation, which may be less efficient when NGF is conjugated to SPIO-Au NPs. SMF-stimulated NGF-SPIO-NPs enhanced β3-tubulin expression, but the upregulation did not outperform DMF. It is hypothesized that DMF creates a rotating magnetic momentum that moves the NPs in and out of the cell, which may promote both intracellular and extracellular Ca²⁺ flux. In contrast, SMF creates a unidirectional magnetic momentum that carries the NPs in one direction and only promotes intracellular Ca²⁺ flux. However, it is still unclear that any additional factors triggered by DMF stimulation of NGF-SPIO-Au NPs could affect the neuronal

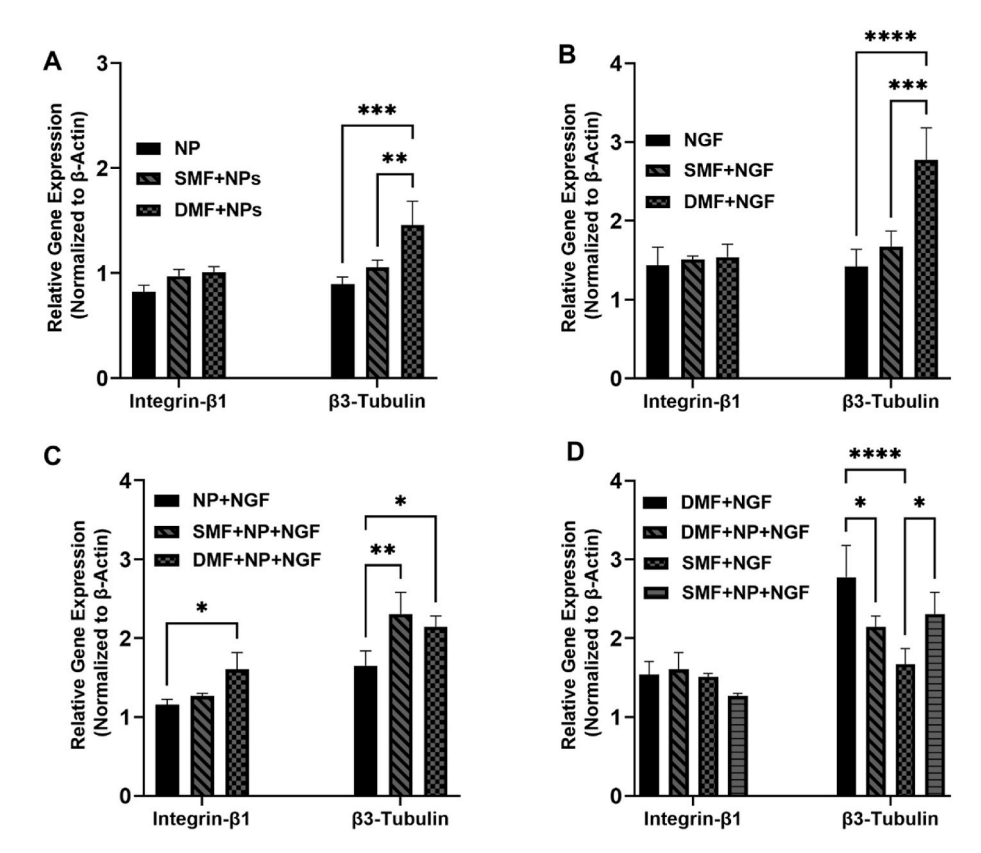


Fig. 8. Relative Gene Expression of neural-specific markers, Integrin- $\beta 1$ and $\beta 3$ -Tubulin, compared to negative control normalized by β -actin. (A) SPIO-Au NPs only, (B) NGF only, (C) NGF-SPIO-Au NPs only, (D) NGF and NGF-SPIO-Au NPs in the presence or absence of SMF and DMF. *P < 0.05, **P < 0.01, ***P < 0.001, ****P < 0.0001.

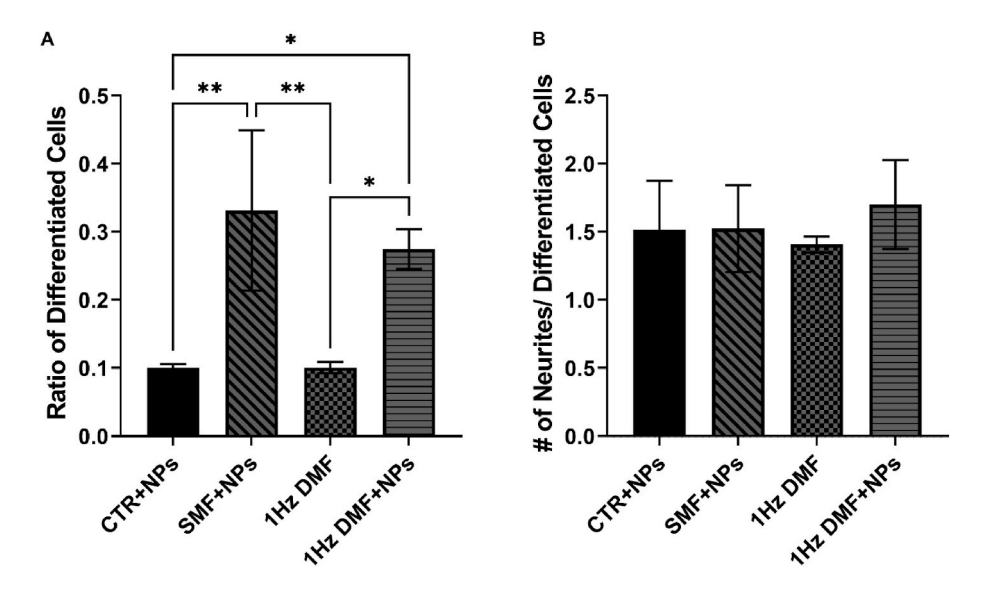


Fig. 9. PC-12 cells differentiation evaluation under different treatments. (A) Ratio of differentiated neuronal cells in total cells (B) Number of neurites per differentiated neuronal cells. $^*P < 0.05$, $^{**}P < 0.01$.

differentiation and regeneration pathway, which will require a more detailed investigation of other neural-related factors to explore further the mechanism of nerve regeneration and differentiation in future studies

In summary, this study reported a novel non-invasive neuroregeneration approach using 1 Hz DMF stimulation integrated with NGF-SPIO-Au NPs, a promising nanomedicine, for promoting neuronal ${\rm Ca}^{2+}$ activity to enhance neuronal differentiation and growth. SMF

stimulation differentially regulated ${\rm Ca^{2+}}$ activity and membrane potential, which resulted in a decreased neuronal differentiation compared to DMF but still had favorable effects compared to no external stimulation. The results demonstrated a promising non-invasive nanomedicine-based neurogenesis technique using DMF-stimulated NGF-SPIO-Au NPs for enhancing nerve regeneration.

Funding

This research was funded by the United States National Science Foundation (NSF) (CAREER Award # CMMI 1851635, Y.W. and GCR awards # ECCS 2021081 (Y.W.) and # ECCS 2020867 (Y-X.O).

Data availability statement

The data presented in this study are available on request from the corresponding author.

CRediT authorship contribution statement

Elias Georgas: performed the experiments and analyzed the results, prepared the manuscript. Muzhaozi Yuan: performed the experiments and analyzed the results, prepared the manuscript. Jingfan Chen: synthesized nanoparticles and designed a magnetic field device. Ya Wang: conceived the idea of this study and were involved in planning and preparation. Yi-Xian Qin: conceived the idea of this study and were involved in planning and preparation, All authors have read and agreed to the published version of the manuscript.

Declaration of competing interest

The authors declare no conflicts of interest.

Acknowledgments

The authors would like to acknowledge Dr. Chung-Chueh Chang of the Thermomechanical & Imaging Nanoscale Characterization Center at Stony Brook University for obtaining the TEM images in this study.

Appendix A. Supplementary data

Supplementary data to this article can be found online at https://doi.org/10.1016/j.bioactmat.2023.01.007.

References

- X.-Z. Chen, et al., Magnetically driven piezoelectric soft microswimmers for neuron-like cell delivery and neuronal differentiation, Mater. Horiz. 6 (7) (2019) 1512–1516, https://doi.org/10.1039/C9MH00279K.
- [2] A. Arranz-Romera, S. Esteban-Pérez, D. Garcia-Herranz, A. Aragón-Navas, I. Bravo-Osuna, R. Herrero-Vanrell, Combination therapy and co-delivery strategies to optimize treatment of posterior segment neurodegenerative diseases, Drug Discov. Today 24 (8) (2019) 1644–1653 (in eng), 2019/08//.
- [3] T. Oda, T. Koike, Magnetic field exposure saves rat cerebellar granule neurons from apoptosis in vitro, Neurosci. Lett. 365 (2) (2004) 83–86.
- [4] R. Cantello, R. Tarletti, C. Civardi, Transcranial magnetic stimulation and Parkinson's disease, Brain Res Brain Res Rev 38 (3) (Feb 2002) 309–327 (in eng).
- [5] A.V. Chervyakov, A.Y. Chernyavsky, D.O. Sinitsyn, M.A. Piradov, Possible mechanisms underlying the therapeutic effects of transcranial magnetic stimulation, Front. Hum. Neurosci. 9 (2015) 303, in eng.
- [6] M. Yuan, Y. Wang, Y.-X. Qin, Promoting neuroregeneration by applying dynamic magnetic fields to a novel nanomedicine: superparamagnetic iron oxide (SPIO)gold nanoparticles bounded with nerve growth factor (NGF), Nanomed. Nanotechnol. Biol. Med. 14 (4) (2018) 1337–1347 (in eng.), 2018/06//.
- [7] C. Riggio, et al., The orientation of the neuronal growth process can be directed via magnetic nanoparticles under an applied magnetic field, Nanomedicine 10 (7) (2014) 1549–1558, in eng.
- [8] Y. Cheng, R.A. Morshed, B. Auffinger, A.L. Tobias, M.S. Lesniak, Multifunctional nanoparticles for brain tumor imaging and therapy, Adv. Drug Deliv. Rev. 66 (2014) 42–57, in eng.
- [9] P. Cherukuri, E.S. Glazer, S.A. Curley, Targeted hyperthermia using metal nanoparticles, Adv. Drug Deliv. Rev. 62 (3) (2010) 339–345, in eng.
- [10] C.S. Kumar, F. Mohammad, Magnetic nanomaterials for hyperthermia-based therapy and controlled drug delivery, Adv. Drug Deliv. Rev. 63 (9) (2011) 789–808 (in eng).
- [11] S.Y. Nam, L.M. Ricles, L.J. Suggs, S.Y. Emelianov, Imaging strategies for tissue engineering applications, Tissue Eng. B Rev. 21 (1) (2015) 88–102 (in eng).
- [12] M. Mahmoudi, H. Hofmann, B. Rothen-Rutishauser, A. Petri-Fink, Assessing the in vitro and in vivo toxicity of superparamagnetic iron oxide nanoparticles, Chem. Rev. 112 (4) (2012) 2323–2338, in eng.

[13] H. Yan, et al., Functional mesoporous silica nanoparticles for photothermal-controlled drug delivery in vivo, Angew Chem. Int. Ed. Engl. 51 (33) (2012) 8373–8377, in eng.

- [14] J. Pinkernelle, V. Raffa, M.P. Calatayud, G.F. Goya, C. Riggio, G. Keilhoff, Growth factor choice is critical for successful functionalization of nanoparticles, Front. Neurosci. 9 (2015) 305 (in eng).
- [15] A.D. Phan, T.X. Hoang, T.H.L. Nghiem, L.M. Woods, Surface plasmon resonances of protein-conjugated gold nanoparticles on graphitic substrates, Appl. Phys. Lett. 103 (16) (2013), 163702.
- [16] H. Arami, A. Khandhar, D. Liggitt, K.M. Krishnan, In vivo delivery, pharmacokinetics, biodistribution and toxicity of iron oxide nanoparticles, Chem. Soc. Rev. 44 (23) (2015) 8576–8607, in eng.
- [17] J.J. Li, N. Kawazoe, G. Chen, Gold nanoparticles with different charge and moiety induce differential cell response on mesenchymal stem cell osteogenesis, Biomaterials 54 (2015) 226–236, in eng.
- [18] D.N. Heo, et al., Enhanced bone regeneration with a gold nanoparticle-hydrogel complex, J. Mater. Chem. B 2 (11) (2014) 1584–1593, in eng.
- [19] Z. Xu, Y. Hou, S. Sun, Magnetic core/shell Fe3O4/Au and Fe3O4/Au/Ag nanoparticles with tunable plasmonic properties, J. Am. Chem. Soc. 129 (28) (2007) 8698–8699, in eng.
- [20] E.E. Connor, J. Mwamuka, A. Gole, C.J. Murphy, M.D. Wyatt, Gold nanoparticles are taken up by human cells but do not cause acute cytotoxicity, Small 1 (3) (2005) 325–327, in eng.
- [21] A. Albanese, W.C. Chan, Effect of gold nanoparticle aggregation on cell uptake and toxicity, ACS Nano 5 (7) (2011) 5478–5489, in eng.
- [22] S. Zhang, Y. Qi, H. Yang, M. Gong, D. Zhang, L. Zou, Optimization of the composition of bimetallic core/shell Fe2O3/Au nanoparticles for MRI/CT dualmode imaging, J. Nanoparticle Res. 15 (11) (2013) 2023, 2013/10/04.
- [23] M. Mahmoudi, S. Sant, B. Wang, S. Laurent, T. Sen, Superparamagnetic iron oxide nanoparticles (SPIONs): development, surface modification and applications in chemotherapy, Adv. Drug Deliv. Rev. 63 (1–2) (2011) 24–46, in eng.
- [24] H. Zhou, F. Zou, K. Koh, J. Lee, Multifunctional magnetoplasmonic nanomaterials and their biomedical applications, J. Biomed. Nanotechnol. 10 (10) (2014) 2921–2949 (in eng).
- [25] H. Maleki, A. Simchi, M. Imani, B.F.O. Costa, Size-controlled synthesis of superparamagnetic iron oxide nanoparticles and their surface coating by gold for biomedical applications, J. Magn. Magn Mater. 324 (23) (2012) 3997–4005, 2012/ 11/01/
- [26] J. Conde, et al., Design of multifunctional gold nanoparticles for in vitro and in vivo gene silencing, ACS Nano 6 (9) (2012) 8316–8324, 2012/09/25.
- [27] M.J. Rak, N.K. Saadé, T. Friščić, A. Moores, Mechanosynthesis of ultra-small monodisperse amine-stabilized gold nanoparticles with controllable size, Green Chem. 16 (1) (2014) 86–89, https://doi.org/10.1039/C3GC41827H.
- [28] K. Chen, H.D. Robinson, Robust dithiocarbamate-anchored amine functionalization of Au nanoparticles, J. Nanoparticle Res. 13 (2) (2011) 751–761, 2011/02/01.
- [29] S.S. Rosenberg, N.C. Spitzer, Calcium signaling in neuronal development, Cold Spring Harbor Perspect. Biol. 3 (10) (2011) a004259, in eng.
- [30] J. Dobson, Remote control of cellular behaviour with magnetic nanoparticles, Nat. Nanotechnol. 3 (3) (2008) 139–143.
- [31] C.J. Meyer, F.J. Alenghat, P. Rim, J.H.-J. Fong, B. Fabry, D.E. Ingber, Mechanical control of cyclic AMP signalling and gene transcription through integrins, Nat. Cell Biol. 2 (9) (2000) 666–668, 2000/09/01.
- [32] R.J. Mannix, et al., Nanomagnetic actuation of receptor-mediated signal transduction, Nat. Nanotechnol. 3 (1) (2008) 36–40, in eng.
- [33] S.R. Ye, J.W. Yang, C.M. Chen, Effect of static magnetic fields on the amplitude of action potential in the lateral giant neuron of crayfish, Int. J. Radiat. Biol. 80 (10) (2004) 699–708, 2004/10/01.
- [34] T. Pashut, et al., Mechanisms of magnetic stimulation of central nervous system neurons, PLoS Comput. Biol. 7 (3) (2011) e1002022.
- [35] J. Ma, et al., Magnetic stimulation modulates structural synaptic plasticity and regulates BDNF-TrkB signal pathway in cultured hippocampal neurons, Neurochem. Int. 62 (1) (2013) 84–91, 2013/01/01/.
- [36] Y. Li, et al., Pulsed electromagnetic field enhances brain-derived neurotrophic factor expression through L-type voltage-gated calcium channel- and Erkdependent signaling pathways in neonatal rat dorsal root ganglion neurons, Neurochem. Int. 75 (2014) 96–104, in eng.
- [37] L.A. Dykman, N.G. Khlebtsov, Uptake of engineered gold nanoparticles into mammalian cells, Chem. Rev. 114 (2) (2014) 1258–1288.
- [38] C.G. England, A.M. Gobin, H.B. Frieboes, Evaluation of uptake and distribution of gold nanoparticles in solid tumors, The European Physical Journal Plus 130 (11) (2015) 1–16.
- [39] S. Zhang, J. Li, G. Lykotrafitis, G. Bao, S. Suresh, Size-dependent endocytosis of nanoparticles, Adv. Mater. 21 (4) (2009) 419–424.
- [40] E.C. Cho, Q. Zhang, Y. Xia, The effect of sedimentation and diffusion on cellular uptake of gold nanoparticles, Nat. Nanotechnol. 6 (6) (2011) 385–391, 2011/06/ 01.
- [41] I. Lynch, T. Cedervall, M. Lundqvist, C. Cabaleiro-Lago, S. Linse, K.A. Dawson, The nanoparticle-protein complex as a biological entity; a complex fluids and surface science challenge for the 21st century, Adv. Colloid Interface Sci. 134–135 (2007) 167–174, 2007/10/31/.
- [42] A. Albanese, P.S. Tang, W.C.W. Chan, The effect of nanoparticle size, shape, and surface chemistry on biological systems, Annu. Rev. Biomed. Eng. 14 (1) (2012) 1–16.
- [43] B.D. Chithrani, J. Stewart, C. Allen, D.A. Jaffray, Intracellular uptake, transport, and processing of nanostructures in cancer cells, Nanomedicine 5 (2) (2009) 118–127 (in eng).

[44] D.B. Peckys, N. de Jonge, Visualizing gold nanoparticle uptake in live cells with liquid scanning transmission electron microscopy, Nano Lett. 11 (4) (2011) 1733–1738 (in eng).

- [45] B.D. Chithrani, W.C. Chan, Elucidating the mechanism of cellular uptake and removal of protein-coated gold nanoparticles of different sizes and shapes, Nano Lett. 7 (6) (2007) 1542–1550, in eng.
- [46] S. Prijic, et al., Increased cellular uptake of biocompatible superparamagnetic iron oxide nanoparticles into malignant cells by an external magnetic field, J. Membr. Biol. 236 (1) (2010) 167–179, in eng.
- [47] I. Venugopal, S. Pernal, A. Duproz, J. Bentley, H. Engelhard, A. Linninger, Magnetic field-enhanced cellular uptake of doxorubicin loaded magnetic nanoparticles for tumor treatment, Mater. Res. Express 3 (9) (2016), 095010, 2016/09/02.
- [48] M. Yuan, Y. Wang, Y.X. Qin, SPIO-Au core-shell nanoparticles for promoting osteogenic differentiation of MC3T3-E1 cells: concentration-dependence study, J. Biomed. Mater. Res. 105 (12) (2017) 3350–3359, in eng.
- [49] J.A. Kim, et al., Enhancement of neurite outgrowth in PC12 cells by iron oxide nanoparticles, Biomaterials 32 (11) (2011) 2871–2877, 2011/04/01/.
- [50] S. Pilakka-Kanthikeel, V.S. Atluri, V. Sagar, S.K. Saxena, M. Nair, Targeted brain derived neurotropic factors (BDNF) delivery across the blood-brain barrier for neuro-protection using magnetic nano carriers: an in-vitro study, in: eng (Ed.), PLoS One 8 (4) (2013), e62241.
- [51] M. Marcus, H. Skaat, N. Alon, S. Margel, O. Shefi, NGF-conjugated iron oxide nanoparticles promote differentiation and outgrowth of PC12 cells, Nanoscale 7 (3) (2015) 1058–1066 (in eng).
- [52] D. Lovisolo, A. Gilardino, F.A. Ruffinatti, When neurons encounter nanoobjects: spotlight on calcium signalling, Int. J. Environ. Res. Publ. Health 11 (9) (2014) 9621–9637, in eng.
- [53] A.E. West, et al., Calcium regulation of neuronal gene expression, Proc. Natl. Acad. Sci. U. S. A. 98 (20) (2001) 11024–11031 (in eng).
- [54] A. Tay, A. Kunze, C. Murray, D. Di Carlo, Induction of calcium influx in cortical neural networks by nanomagnetic forces, ACS Nano 10 (2) (2016) 2331–2341, 2016/02/23.

- [55] A. Tay, D. Di Carlo, Magnetic nanoparticle-based mechanical stimulation for restoration of mechano-sensitive ion channel equilibrium in neural networks, Nano Lett. 17 (2) (2017) 886–892, 2017/02/08.
- [56] C. Grassi, et al., Effects of 50Hz electromagnetic fields on voltage-gated Ca2+ channels and their role in modulation of neuroendocrine cell proliferation and death, Cell Calcium 35 (4) (2004) 307–315, 2004/04/01/.
- [57] A. Özgün, A. Marote, L.A. Behie, A. Salgado, B. Garipcan, Extremely low frequency magnetic field induces human neuronal differentiation through NMDA receptor activation, J. Neural. Transm. 126 (10) (2019) 1281–1290, in eng.
- [58] J.M. Kanczler, et al., Controlled differentiation of human bone marrow stromal cells using magnetic nanoparticle technology, Tissue Eng. 16 (10) (2010) 3241–3250, in eng.
- [59] L. Nikolić, D. Bataveljić, P.R. Andjus, M. Nedeljković, D. Todorović, B. Janać, Changes in the expression and current of the Na+/K+ pump in the snail nervous system after exposure to a static magnetic field, J. Exp. Biol. 216 (Pt 18) (2013) 3531–3541, in eng.
- [60] R.R. Arvizo, et al., Effect of nanoparticle surface charge at the plasma membrane and beyond, Nano Lett. 10 (7) (2010) 2543–2548 (in eng).
- [61] M.J. McLean, R.R. Holcomb, A.W. Wamil, J.D. Pickett, A.V. Cavopol, Blockade of sensory neuron action potentials by a static magnetic field in the 10 mT range, Bioelectromagnetics 16 (1) (1995) 20–32 (in eng).
- [62] H.Y. Nam, et al., Cellular uptake mechanism and intracellular fate of hydrophobically modified glycol chitosan nanoparticles, J. Contr. Release 135 (3) (2009) 259–267, 2009/05/05/.
- [63] R. Piacentini, C. Ripoli, D. Mezzogori, G.B. Azzena, C. Grassi, Extremely low-frequency electromagnetic fields promote in vitro neurogenesis via upregulation of Cav1-channel activity, J. Cell. Physiol. 215 (1) (2008) 129–139.
- [64] Z.C. Sun, et al., Extremely low frequency electromagnetic fields facilitate vesicle endocytosis by increasing presynaptic calcium channel expression at a central synapse, Sci. Rep. 6 (2016), 21774 (in eng).